Aquarius: An Instrument to Monitor Sea Surface Salinity from Space

D.M. Le Vine
Goddard Space Flight Center, Greenbelt,MD
G.S.E. Lagerloef
Earth and Space Research, Seattle, WA
R. Colomb
Comisión Nacional de Actividades Espaciales (CONAE), Buenos Aires, AR
S. Yueh
Jet Propulsion Laboratory, Pasadena, CA
F. Pellerano
Goddard Space Flight Center, Greenbelt,MD

ABSTRACT - Aquarius is a combined passive/active L-band microwave instrument being developed to map the salinity field at the surface of the ocean from space. The data will support studies of the coupling between ocean circulation, the global water cycle and climate. Aquarius is part of the Aquarius/SAC-D mission, a partnership between the USA (NASA) and Argentina (CONAE) with launch scheduled in 2009. The primary science objective of this mission is to monitor the seasonal and interannual variation of the large scale features of the surface salinity field in the open ocean with a spatial resolution of 150 km and a retrieval accuracy of 0.2 psu globally on a monthly basis.

I. INTRODUCTION

Aquarius is a combined active/passive L-band microwave instrument designed to map the surface salinity field of the oceans from space. It will be flown on the Aquarius/SAC-D mission, a partnership between the USA space agency (NASA) and Argentine space agency (CONAE) with launch scheduled for 2009. The mission is composed of two parts: (a) Aquarius, a radiometer/scatterometer instrument combination for measuring sea surface salinity, which is being developed by NASA as part of the Earth System Science Pathfinder (ESSP) program; and (b) SAC-D, which is the fourth spacecraft service platform in the CONAE Satelite de Aplicaciones Cientificas (SAC) program and includes several additional instruments. The primary focus of the mission is to monitor the seasonal and interannual variations of the salinity field in the open ocean. The mission also meets the needs of the Argentine space program for monitoring the environment and for hazard detection. The objective of this paper is to give an overview of the mission and a description of the Aquarius instrument package. For information on a related mission, SMOS, being developed in Europe see [1, 2].

II. SALINITY SCIENCE OBJECTIVES

A. Aquarius Science Objectives

The primary objective of the Aquarius instrument development is to provide information to study the interactions between the water cycle (marine rainfall and evaporation, melting and freezing of ice, and river runoff), ocean circulation, and the climate. This requires monitoring the seasonal and interannual variation of the large scale features of the sea surface salinity (SSS) field in the open ocean with an accuracy of 0.2 psu (Practical Salinity Scale [3]) or less. For example, salinity modulates the large scale thermohaline circulation, driven by buoyancy, which moves large masses of water and heat around the globe and maintains the present climate. Of the two variables that determine buoyancy (salinity and temperature), temperature is already being monitored (e.g. [4]). The salinity field is the missing variable needed to understand this circulation.

Salinity also plays an important role in energy exchange between the ocean and atmosphere. In addition to the thermohaline circulation, in areas of strong precipitation, fresh water "lenses" can form on the surface [5]. These are buoyant layers of water that form stable layers and insulate the water in the mixed layer below from the atmosphere [6]. This alters the air-sea coupling (energy exchange) and can affect the evolution of tropical intra-seasonal oscillations, monsoons and the El Nino-Southern Oscillation (ENSO). Ocean-atmosphere water fluxes dominate the global hydrologic cycle, accounting for 86% of global evaporation and 78% of global precipitation [7]. Changes in surface salinity reflect changes in surface freshwater forcing. Systematic mapping of the global salinity field will help to reduce the wide uncertainties in the marine freshwater budget [8] and better understand the global water cycle and how it is changing.

The time and spatial scale of observations needed to improve understanding of these processes are relatively long but the salinity changes are relatively small (tenths of a psu) compared, for example, to processes in the coastal ocean. The goal for the Aquarius instrument is to provide global maps of the sea surface salinity field in the open ocean on a monthly basis with an average accuracy of 0.2 psu and at a spatial resolution of 150 km. In comparison, the existing database is too sparse in both time and space to resolve key processes. For example, dividing the ice-free ocean into one-degree squares in latitude and longitude, one finds that about 25% has never been sampled and more than 73% has fewer than 10 samples [9, 10]. The sparse data is primarily a reflection of the limitations of in situ sampling. Aquarius will record more SSS observations in two months than have been measured since such observations began about 125 years ago.

B. Remote Sensing Heritage

Research in the 1970's at NASA's Langley Research Center [11] and later at the Goddard Space Flight Center [12] demonstrated that sea surface salinity can be measured remotely with a passive microwave sensor. Salinity modulates the thermal emission from sea water at a level that is measurable when observed at the long wavelength end of the microwave spectrum. This is illustrated in Figure 1 which shows the observable parameter (brightness temperature, T_B) as a function of water temperature for constant values of salinity. These curves are for an ideal surface (no waves) when looking perpendicular to the surface (nadir) and were computed using the model developed by Klein and Swift [13] for the dielectric constant of sea water at L-band. In the remote sensing approach adopted for Aquarius, the sensor measures T_B (vertical axis) and

sea surface temperature (SST) is obtained from an ancillary source (e.g. maps derived from satellite sensors).

The range of salinity and temperature to be encountered in the open ocean is indicated by the shaded area in Figure 1. The associated change in brightness temperature is small but measurable with modern radiometers. The window at 1.413 GHz (L-band) set aside for passive use only, where Aquarius will operate, is an optimum choice for remote sensing of salinity and is very near the peak in sensitivity of brightness temperature, T_B, to changes in salinity. On the other hand, when actually making the remote sensing measurement from space, there are a number of complicating issues that must be taken into account. For example, surface roughness (e.g. waves) can also cause changes in the observed brightness temperature with an order of magnitude comparable to the salinity signature [14]. Aquarius includes a scatterometer to help correct for this effect. The scatterometer (backscatter) responds directly to surface roughness, and in the design of Aquarius, the radiometer and scatterometer operate at nearly the same frequency and will share the same antenna feed and look at the same pixel with approximately the same footprint. The approach is based on experiments at the Jet Propulsion Laboratory with the passive/active L-band instrument PALS [15, 16]. Another issue to be taken into account is Faraday rotation (rotation of the polarization vectors as the radiation propagates from the surface through the ionosphere) which can be significant at L-band [17]. The inversion from brightness temperature to salinity depends (except at nadir) on polarization. To help correct for this potential source of error, the radiometer in Aquarius will include a polarimetric channel and will use the measured third Stokes parameter and an algorithm suggested by Yueh [18] to retrieve the angle of polarization rotation. Finally, the sun is a significant source of radiation at L-band [19] and to avoid reflection from the ocean surface into the main beam of the antenna, the mission will be in a sun-synchronous orbit near the day-night terminator (i.e. 6 am/6 pm equatorial crossing) with the antenna beams pointing toward the night time side of the orbit. A review of the issues associated with remote sensing of SSS from space has been given by [20].

III. AQUARIUS/SAC-D MISSION

The mission is composed of two parts, the Aquarius instrument which is being provided by NASA and the SAC-D spacecraft service platform and associated instruments which is being provided by CONAE. Specifically, CONAE will provide the spacecraft bus (SAC-D), a complement of instruments, and the communications link and telecommunications for mission command, control and science data acquisition. Table I is a list of the additional instruments provided by CONAE [21]. They include the New InfraRed Scanner Technology (NIRST) camera (developed jointly with the Canadian Space Agency) to detect forest fires, and a high sensitivity Optical Camera and the Data Collection System. CONAE is also developing a microwave radiometer (MWR) that will provide measurements of rain, ocean surface wind (speed and direction) and sea-ice. The MWR consists of separate radiometers at 23.8 and 36.5 GHz. Each radiometer operates in pushbroom mode with eight beams (i.e. a reflector with eight feed horns) providing a swath width of 390 km and a resolution of 50 km. The system at 36.5 GHz is polarimetric (V and H polarization plus the third Stokes parameter) and the radiometer at 23.8 Ghz measures vertical polarization only. Each system employs one detector which scans the eight feeds with an estimated sensitivity of 0.5 K. The plan is to orient this instrument so as to image the Aquarius swath to complement as much as possible the Aquarius measurements (for

example, to assist in the development of a rain flag). Also included among the instruments on SAC-D is a GPS atmospheric occultation experiment called ROSA, which will be provided by the Italian Space Agency (ASI) and the ICARE/ SODAD instrument called, CARMEN1, provided by the French Centre National d'Etudes Spatiales (CNES) to measure the radiation and micro-particle environment in space.

Aquarius and the suite of instruments on SAC-D address goals of the Argentine space agency to contribute to the understanding of the total Earth system and the effects of natural and human-induced changes on the global environment. The measurements address the Argentina Space Information Cycle II "Information System devoted to Oceanography, the Coastal Environment, Climate and Hydrology" and Space Information Cycle III "Emergency Management" as set forth in the "National Space Program, Argentina in Space 2004-2015". Among the emergency management issues are natural and man-made events such as forest and pasture fires, floods, volcanic eruptions, and severe weather (tornados, cyclones, hurricanes). Among the applications in Cycle II are studies of the Southern Atlantic Ocean, the Antarctic Sea and other geographic regions to allow for the seasonal forecast of global phenomena such as El Niño as well as the measurement of related parameters such as soil moisture (support for agricultural and livestock management) and sea and coast surveys for scientific purposes as well as for the support of harbor, transportation and navigation activities.

Figure 2 illustrates the mission and roles and responsibilities of the partners and Table II summarizes the mission parameters. The launch (provided by NASA) is from NASA's Western Test Range at Vandenberg AFB using a Boeing Delta-II launch vehicle (also provided by NASA). The observatory will go into a sun-synchronous orbit at an altitude of 657 km, an inclination of 98 degrees and equatorial crossing times of 6 am (descending) and 6 pm (ascending). The orbit is a 7-day exact repeat orbit. The Aquarius swath (390 km) and orbit have been selected so that complete global sampling is obtained during each 7-day period. However, the final Aquarius data product will be a monthly map of the salinity field. The 7-day orbit has been selected to provide timely sampling (one sample at least every 7 days) together with additional averaging (several samples per resolution cell) to help reduce noise to better meet the goal of 0.2 psu (RMS on a global average basis).

The Aquarius instrument consists of radiometer at 1.413 GHz and scatterometer at 1.26 GHz. The radiometer (Section IVB) is the primary instrument for measuring sea surface salinity and the scatterometer (Section IVC) is being carried to provide a correction for surface roughness, the largest unknown in the retrieval algorithm. Development of the Aquarius instrument package is a partnership within NASA of the Goddard Space Flight Center (GSFC) and the Jet Propulsion Laboratory (JPL). GSFC is responsible for the radiometer and ground science data processing system, while JPL is responsible for the scatterometer, instrument integration and test and pre-launch mission management.

After launch, GSFC takes over management of the science and instrument operations. CONAE will provide the ground station and telecommunication services at their ground station and Mission Operations Center (MOC) in Cordoba, Argentina. Aquarius science telemetry will be separated at the MOC and sent to the Goddard Space Flight Center for processing. The salinity data products will be generated at GSFC and eventually will be sent to the Physical

Oceanography Distributed Active Archive Center (PO.DAAC) at JPL for permanent archiving. Salinity maps and relevant ancillary data will be released to the public from GSFC prior to final archiving.

IV. THE AQUARIUS INSTRUMENT

A. The Antenna Structure

Perhaps the most prominent feature of the Aquarius instrument is the antenna, a 2.5-m offset parabolic reflector with three feed horns. The three beams are arranged to image in pushbroom fashion pointed across track (roughly 90 degrees with respect to the spacecraft heading) at look angles between 25 and 40 degrees with respect to the satellite nadir. This is illustrated in Figure 3 which shows (top) the spacecraft and the look-angle, θ. The spacecraft flies into the page with the sun at the left and the three beams pointing toward the right at angles $\theta =$ 25.8, 33.8 and 40.3 degrees which correspond to local incidence angles at the surface of 28.7, 37.8 and 45.6 degrees, respectively. The footprint of the three beams on the surface is illustrated on the bottom of Figure 3. The resolution of the three radiometer beams ranges from 76 x 94 km for the inner beam to 97 x 157 km for the outer beam and together they provide coverage of a swath of about 390 km. The three beams do not point exactly across track: the inner and outer beam point slightly forward and the middle beam (33.8 degrees) points slightly aft. The feed for each beam is shared by both the radiometer and scatterometer. The dashed line in Figure 3 (bottom) shows the resolution cell (3 dB level in the footprint) for the scatterometer. There are three radiometers (each feed has a dedicated radiometer); however, there is only one scatterometer which cycles among the three feeds as described in Sections B and C below. The scatterometer and radiometer beams are aligned at the beam center and have approximately the same shape at the 3dB level as indicated in the figure.

In Figure 4, Aquarius is shown in its stowed configuration (left) and deployed (right). The parabolic reflector is deployed with a single fold mechanism and is the largest size that could fit inside the Delta-II launch vehicle fairing without a fold. The difficulty with remote sensing at the low frequency end of the microwave spectrum is the size of the structures needed to obtain even the modest spatial resolution attempted with Aquarius (150 km). The stowed observatory (Aquarius plus service platform) is 4.85 m from top to bottom and the stowed Aquarius alone is 2.3 m tall. The collar at the junction between Aquarius and the service platform (SAC-D) is a sun shield. It is part of the thermal control for the radiometers (to help keep IR radiation from the sun off the electronics). Tight thermal control ($<0.1^{o}$ C over 7 days) is an important design requirement of this instrument and is needed to achieve the final accuracy (0.2 psu). The sun is also a source of radiation at L-band [19, 20], but a complete RF shield was ruled out because of the potentially large size needed to be effective.

Figure 5 shows the feed assembly in more detail. At the top is a view of one of the individual feeds and at the bottom is a view (from the back) of the entire feed assembly. The feed horn itself is a choked, circular waveguide horn with an aperture of about 0.5 meters. Each feed is connected to an OMT through a thermal isolator. The OMT separates vertical and horizontal polarization. The feeds are clocked (oriented with respect to the reflector) to obtain horizontal and vertical polarization at the Earth surface as conventionally defined in radiometry. One of the

ports of the OMT can be seen at the bottom rear in image at the top of Figure 5. The radiometer electronics will be mounted at the top of this structure together with a heater and radiator plate which are part of the thermal control. The radiometer RF function is isolated from the scatterometer by diplexers (one for each polarization) which are the large rectangles on each side of the OMT. Couplers where the correlated noise diode (see the Section IV.B) is injected for calibration of the polarimetric operation of the radiometer can be seen just behind the diplexer.

B. The Radiometer

The radiometers are Dicke radiometers that use noise injection for calibration. A critical requirement in the design of these radiometers is long-term (days) stability. Stability is critical because significant averaging must be done to achieve the Aquarius goal for an accuracy of 0.2 psu (gobal rms on a monthly basis). Since it will take 7 days to map the globe, the radiometers must be stable over at least 7 days. The design requirement set for Aquarius is that the radiometers be stable to within 0.13 K over 7 days. A primary element in maintaining stability is adequate internal calibration and good thermal control. The design adopted for the Aquarius radiometers is based on research conducted under NASA's Instrument Incubator Program [22] that uses two internal reference sources (noise diode and Dicke load).

The radiometer is divided into several elements as shown in Figure 5 (top) and Figure 6. Beginning at the OMT, these elements are the OMT Couplers, the Correlated Noise Diode (CND), two diplexers (one for each polarization), the Radiometer Front End (RFE), the Radiometer Back End (RBE), and the Digital Processing Unit (DPU). The OMT Couplers, CND, diplexers, and RFE are mounted on the OMT as shown at the top of Figure 5 (the CND is hidden beneath the RFE). Thermal control of these elements is critical to obtaining the radiometric stability needed for successful retrieval of salinity at the accuracy desired for Aquarius. To achieve this, the OMT assembly is cold-biased passively by means of radiator plates and appropriate coatings and controlled actively using heaters mounted to the assembly. The design requirement is to control the thermal environment of the RFE to change less than 0.1^{o} C over 7 days.

A functional block diagram for the radiometer is shown in Figure 6. The primary amplification is done in the radiometer front ends (RFE). There is a separate RFE for each feed assembly. In the RFE, the two signals from the OMT (one for vertical polarization and one for horizontal polarization) are amplified and then combined to form four channels (vertical, horizontal and the sum and difference which is equivalent polarization at ±45 degrees). The sum and difference signal will be used to compute the third Stokes parameter (i.e. detected with a square-law detector in the RBE and later subtracted during the ground processing). The first elements at the input of the RFE are the Dicke switch and its reference load followed by a coupler to a noise diode that provides the hot load. Together, these are the references used for internal calibration. These calibration references are at the heart of the radiometer performance and tight thermal control is needed to meet the required radiometric performance. In order to meet the required performance, the radiometric temperature of the Dicke load must be known with an uncertainty of < 50 mK, and the coupled noise temperature must be stable to < 300 ppm. These parameters, together with the thermal control mentioned above, have been shown to be adequate to achieve the required radiometric stability (0.13K over 7 days [22]). Also, this radiometer architecture is

largely implemented using microstrip-based technology, a trade-off made to reduce size and improve thermal control (at the expense of increased loss).

Between the OMT and the RFE are the OMT coupler and the diplexers (Figure 6). The OMT coupler provides a port for injecting signal from a second noise diode, the Correlated Noise Diode (CND). This signal is used to monitor the phase and amplitude balance between the channels, a calibration that is necessary for proper polarimetric performance and calculation of the third Stokes parameter. The diplexers are devices that allow the scatterometer and radiometer to use the same feed horn assembly without damage to the radiometer electronics. They are cavity type filters that provide enough rejection to guarantee no damage to the radiometer from the scatterometer pulse. To provide additional isolation, whenever the scatterometer transmits, the Dicke switches are switched to the reference load. The total isolation (diplexer plus switch) prevents any active component in the RFE from being saturated by the scatterometer.

The radiometer back end (RBE) contains additional amplification, band-pass filtering, and the detectors for each channel (Figure 6). Its performance (stability) is less critical to the overall stability of the radiometer system because it is located behind all the calibration sources and after the first stage gain in the RFE. The design requirement for temperature control of the RBE is a maximum change of 0.4 C (rms) over 7 days. Because less control is necessary, the RBE has been physically separated from the more critical elements mounted on the OMT. This will facilitate thermal control of this more sensitive group.

The final stage of the radiometer is the digital processing unit (DPU). The detected signals from each radiometer channel are digitized in the RBE using voltage-to-frequency converters (VFC). These devices output pulses whose frequency is proportional to the detected signal. These pulses are counted asynchronously, and the frequency determined, by the DPU. The DPU also houses the radiometer controller and collects temperature and housekeeping data.

Figure 7 shows the timing diagram for the hardware. The fundamental timing unit is 10 ms (approximately 1 ms for the scatterometer transmit pulse and 9 ms of observation time for the radiometer). The radiometer and scatterometer operation are alternated so that the two sensors look at the same piece of ocean nearly simultaneously. The three radiometers (one for each beam) operate in parallel. During 120 ms each radiometer collects 7 samples (9 ms long and repeated each 10 ms) looking into the antenna followed by 5 samples devoted to the calibration sources (two noise diodes and Dicke load). This 120 ms sequence is then repeated. However, because of limitations with the on-board data storage, not all of this data will be downloaded. It is planned to average two pair of the 10 ms antenna looks and transmit to ground three samples at the 10 ms resolution followed by two at 20 ms. The samples of the calibration references transmitted to the ground will be the average of 10 samples.

The switching sequence between antenna, Dicke load, and noise diodes has been optimized to maximize antenna observations and minimize Noise Equivalent Delta Temperature (NEDT). This optimization is based on the requirement that the radiometer gain and receiver temperature are relatively stable quantities. Therefore, the duty cycle of the calibration observations can be reduced to be consistent with the time constant of these parameters. The stable values needed for

calibration are obtained by averaging over longer periods. The effect of this approach is a significantly higher duty cycle for the antenna (i.e., ocean) observations with an improved NEDT compared to the standard approach using equal duty cycles [22]. The goal is for a NEDT ≤ 0.08 K in 5.76 seconds. The design performance for NEDT is about 0.06K.

The radiometer has also been designed to include precautions against Radio Frequency Interference (RFI). A study conducted by NASA and ITT looked at potentially damaging sources, as well as interference that would impact the science retrieval [23]. The primary source of interference for the radiometer is ground-based air surveillance radars. The level of interference is a function of out-of-band emissions from these radars and also a function of the rejection level of radiometer filters in the skirts where the radar band is located (i.e. where the radar is permitted to transmit). The findings of the study suggested a three-tiered approach. The first step is to include 2 watt limiters to protect the low noise amplifiers (LNA) in the RFE against worst case damage. The second approach is to sample at a sufficiently high rate to facilitate identification of RFI with the ability to remove it without complete loss of data. The study suggested that the radiometer data should not be averaged more than about 30 ms before download. The current design calls for most data to be down loaded at 10 ms sample rate and some at 20 ms. Finally, the radiometer band-limiting filters (located in the RBE) were designed to reduce the potential interference to a probability of <1% over the ocean. In terms of filter parameters, this requirement is equivalent to a 25 MHz bandwidth, 7-pole Chebyshev filter. This is achieved with several filter stages. These include the diplexer and the two band pass filters in the RBE before the detector (Figure 6).

C. The Scatterometer

Although Aquarius will have three separate radiometers, it will have only one scatterometer which sequences among the three feeds and two polarizations. The operation is synchronized so that the two instruments monitor the same ocean pixel at essentially the same time as shown in the timing diagram (Figure 7). First, the scatterometer transmits a 1 ms pulse with 100 Hz Pulse Repetition Frequency (PRF), which results in 10 ms between pulses and a timing sequence in which scatterometer pulses and radiometer observations alternate. Secondly, the scatterometer alternately transmits at horizontal polarization (H) and receives at vertical polarization (V), receives at V but noise only (to calibrate the background noise), and then transmits at V and receives at V polarization. Then this is repeated with the polarizations reversed: transmitting at V and receiving at H polarization, then receiving at H polarization but noise only, and finally transmitting and receiving at H polarization. When this cycle of measurements at four polarization steps and two noise-only steps is completed at one beam (feed horn), the scatterometer signal is moved to the next beam and the cycle is repeated. This is done via a switching network at the output of the scatterometer front end (see SFE in Figure 8). With this sequence, the scatterometer will measure power (only power and no phase information) at VV, HV, VH and HH polarization combinations at each feed. The plan is to record data in all 4 polarizations but to use the total power (VV + HH + VH + HV), which is insensitive to the Faraday rotation, to retrieve the roughness correction for the radiometer. A complete switching cycle over 3 antenna beams takes 18 pulse steps with 12 for echo measurements and 6 for noise only measurements. The time to complete one full scatterometer switching cycle is 0.18 seconds. In 0.72 s, the radiometer will have completed 6 full cycles and the scatterometer 4 full cycles.

Notice that the radiometer and scatterometer are receiving signal at the same time. During the 1 ms scatterometer transmit interval, the radiometer is protected by the diplexer and by blanking the radiometer input (switching to a calibration load). During the ensuing 9 ms the radiometer is isolated from the scatterometer backscatter by the diplexer and the band pass filters in the RBE (last paragraph in Section IVB above). There is sufficient isolation between the two frequencies that any leakage of the backscatter into the radiometer is negligible.

The scatterometer electronics are divided into five boxes, including the Scatterometer Front End (SFE), Scatterometer Backend (SBE), Scatterometer Chirp Generator (SCG), Solid State Power Amplifier (SSPA) and Low Voltage Power Supply (LVPS). The scatterometer electronics will receive the timing signals from the Instrument Command and Data Subsystem (ICDS) and will send radar echoes down-converted to baseband frequencies back to the ICDS for digitization, power accumulation, averaging and time-tagging. The scatterometer electronics is housed on the feed main support frame (bottom of Figure 5) together with the radiometer back end (RBE) and except for the diplexer is separate from the thermally sensitive components on the OMT unit.

The first element at the input to the scatterometer front end is the 7-position switch which allows the single scatterometer to transmit in vertical (V) or horizontal (H) polarization sequentially at each of the feeds (Figure 8). The output of the switch is connected via cables to the appropriate diplexer on the OMT-feed structure (top, Figure 5). The SFE also includes a calibration loop which is an essential part of the design to enable accurate on-orbit calibration of transmit power and receiver gain. The use of a calibration loop has been employed in several recent spaceborne radars, including the JPL Shuttle Imaging Radar-C, SeaWinds scatterometers, and airborne radars such as the Passive/Active L-band (PALS) instrument and the Polarimetric Scatterometer, POLSCAT, [16]. The SFE calibration loop consists of a coupler through a path with high attenuation to leak a small portion of the radar transmit energy into the receiver during each transmit pulse. This signal is coupled into the receive path in the SFE just after the front end switch. This small leakage signal is proportional to the product of transmit power and receiver gain and is used to calibrate the radar echoes from the surface. The SFE also includes a band pass filter to help suppress RFI (largely interference from other radars). Surprisingly, this is potentially a greater problem for the scatterometer than the radiometer, especially over land where there are many radars and no “protected” band [23].

From the SFE the radar signal is passed to the SBE where it is processed to baseband. The SBE includes amplifiers, bandpass filters and mixers to convert the radar echoes to baseband at 4 MHz. Power detection is performed in the ICDS with analog-to-digital (A/D) conversion, voltage squaring and accumulation. To insure that the calibration loop signal is in the dynamic range of the SBE and ICDS, the SBE includes a step attenuator following the low noise amplifier. The step attenuator will be switched to low insertion loss (about 2 dB) during the range gate window for echoes and will be flipped to high insertion loss (about 50 dB) during transmit for the calibration loop signals. The SBE also include an 8-MHz Stable Local Oscillator (STALO), frequency mutipliers, mixers and bandwidth filters, along with the chirp signal with 4MHz bandwidth from the SCG, to generate the signal at 1.26 GHz, which is used to excite the SSPA for high power on transmission.

In addition to the use of the calibration loop, high accuracy (0.1^{o} deg C) temperature sensors will be deployed on temperature-sensitive components. The goal is to achieve better than 0.1 dB calibration stability after corrections for changes in temperature. The allocation is a calibration stability accuracy of 0.05 dB for the electronics enclosed in the calibration loop and 0.09 dB for the total loss of components between the SFE and the antenna feed. The thermal design is to use passive control to keep the temperature of the electronics within about 1^{o} C. This is tight temperature control, although much less stringent than the thermal control needed for the radiometers. It will keep the change of the total electronics loss to about 0.3 to 0.4 dB. To calibrate the temperature dependence of these various electronics components, pre-launch calibration tests will be conducted to characterize the loss of the calibration loop, step attenuator, beam-select switch and other critical elements as a function of temperature. This will permit corrections to be made. The goal is to ensure that the residual calibration stability error is much less than 0.1 dB after the effects of temperature drift are corrected.

V. SUMMARY

Aquarius is a combined passive/active L-band microwave instrument that will be flown as part of the Aquarius/SAC-D mission to map the surface salinity field of the oceans from space. The goal is to monitor the seasonal and interannual variation of the large scale features of the surface salinity field in the open ocean with a spatial resolution of 150 km and a retrieval accuracy of 0.2 psu globally on a monthly basis. Salinity is the missing variable needed to understand the thermohaline circulation of the oceans, and the data provided by Aquarius will permit expanded understanding of the coupling between ocean circulation, the global water cycle and climate. The impact of Aquarius will be dramatic: Aquarius will record more SSS observations in two months than have been measured since such observations began about 125 years ago.

VI. ACKNOWLEDGMENT

The work described in this paper that was performed by the Jet Propulsion Laboratory was carried out under a contract with the National Aeronautics and Space Administration. Also, the work described here reflects the contribution of members of a large Aquarius project team. The authors are grateful to the many other Aquarius team members who have contributed to the overall mission design and preparation of technical information.

VII. REFERENCES

1. Y. Kerr et al.: "Soil Moisture Retrieval from Space: The Soil Moisture and Ocean Salinity (SMOS) Mission", IEEE Trans. Geosci. and Remote Sens., Vol. 39 (# 8), August, 2001.
2. Y.H. Kerr, P. Waldteufel, J.-P. Wigneron, J. M. Martinuzzi, B. Lazard, J.-M. Goutoule, C. Tabard and A. Lannes, “The soil moisture and ocean salinity mission: an overview” in **Microwave Radiometry and Remote Sensing of the Earth’s Surface and Atmosphere**, Pampaloni P. and S. Paloscia, Eds., VSP, The Netherlands, pp. 467-475, 2000.
3. Lewis, E.L., “The Practical Salinity Scale 1978 and its antecedents”, IEEE J. Oceanic Eng., OE-5, -8, 1980.

4. Gentemann, C.L, F.J. Wentz, C.M. Mears, and D.K. Smith., "In-situ validation of TRMM microwave sea surface temperatures", *Journal of Geophysical Research*, 109: C04021, 2004.
5. Sprintall, J. and M. Tomzcak, "Evidence of the barrier layer in the surface layer of the tropics", J. Geophys. Res., 97, 7305-7316, 1992.
6. Lukas, R. and E.R. Lindstrom, "The mixed layer of the Western Equatorial Pacific Ocean", Geophys. Res., 96 (suppl.), 3343-3357, 1991.
7. Schmitt, R.W., "The ocean freshwater cycle", JSC Ocean Observing System Development Panel, Texas A&M University, College Station, Texas, 40pp, 1994.
8. Johnson, E. S., G. S. E. Lagerloef, J. T. Gunn, and F. Bonjean, 2002. Salinity advection in the tropical oceans compared to atmospheric freshwater forcing: a trial balance, J. Geophys. Res., 10.1029/2001JC001122.
9. Koblinsky, C.J., P. Hildebrand, D. Le Vine and F. Pellerano, "Sea surface salinity from space: Science goals and measurement approach", Radio Science, 38 (#4), 8024, doi:10.1029/2001RS002584, March, 2003.
10. Lagerloef, G.S.E, C. Swift, D. Le Vine, "Sea surface salinity: The next remote sensing challenge", Oceanogr. 8, 44-50, 1995.
11. Blume, H-J C., B.M. Kendall and J.C. Fedors, "Measurements of ocean temperature and salinity via microwave radiometry", Boundary Layer Met., 13, 295, 1978.
12. Le Vine, D.M., M. Kao, R. Garvine and T. Sanders, "Remote sensing of ocean salinity: Results from the Delaware Coastal Current experiment", J. Atmos. Oceanic Tech. 15, 1478-1484, 1998.
13. Klein, L.A. and C.T. Swift, "An improved model for the dielectric constant of sea water at microwave frequencies", IEEE Trans. Antennas and Propag., AP-25, 104-111, 1977.
14. Camps, A.; Font, J.; Vall-llossera, M.; et al., "The WISE 2000 and 2001 field experiments in support of the SMOS mission: sea surface L-band brightness temperature observations and their application to sea surface salinity retrieval", IEEE Trans. Geosci. Remote Sens., 42 (#4),804 – 823, 2004.
15. Wilson, W.J.; Yueh, S.H.; Dinardo, S.J.; Chazanoff, S.L.; Kitiyakara, A.; Li, F.K.; Y. Rahmat-Samii, "Passive active L- and S-band (PALS) microwave sensor for ocean salinity and soil moisture measurements," IEEE Trans. Geosci and Remote Sensing, 39 (# 5),1039-1048, 2001.
16. Yueh, S.H., W. J. Wilson, and S. Dinardo, "Polarimetric radar remote sensing of ocean surface wind", IEEE Trans. Geosci. Remote Sens., 40, 793-800, April 2002.
17. Le Vine, D.M. and S. Abraham, "The effect of the ionosphere on remote sensing of sea surface salinity from space: Absorption and emission at L-band", IEEE Trans. Geosci. Remote Sens., 40 (#4), 771-782, 2002.
18. Yueh, S.H., "Estimates of Faraday rotation with passive microwave polarimetry for microwave remote sensing of Earth surfaces", IEEE Trans. Geosci Remote Sens., Vol 38 (#5), pp 2434-24-38, 2000.
19. Le Vine, D.M., S. Abraham, F. Wentz, G.S.E. Lagerloef, "Impact of the Sun on remote sensing of sea surface salinity from space", Proc. Internat. Geosci. & Remote Sens. Sympos, Seoul, S. Korea, July, 2005.
20. Yueh, S.H., R. West, W.J. Wilson, F.K. Li, E.G. Njoku, and Y. Rahmat-Samii, "Error sources and feasibility for microwave remote sensing of ocean surface salinity", IEEE Trans. Geosci and Remote Sensing, Vol 39, #5, pp 1049-1059, May, 2001.

21. Sen, A. Y. Kim, D. Caruso, G. Lagerloef, R. Colomb, D. Le Vine and S. Yueh, "Aquarius/SAC-D Mission Overview", Proc SPIE Remote Sensing, Conf 6361-4; Stockholm, Sweden, 11-14 Sept. 2006
22. Wilson, W. J., Tanner, A., Pellerano, F., and Horgan, K., "Ultrastable radiometers for future sea surface salinity missions", Jet Propulsion Laboratory Report D-31794, April 2005.
23. Piepmeier, J.R., Pellerano, F.A., Freedman, A., "Mitigation of terrestrial radar interference in L-band spaceborne microwave radiometers", to appear in International Geoscience and Remote Sensing Symposium, IGARSS06, Denver, CO, July, 2006

TABLE I
SAC-D Instruments

Instrument	Objective	Description	Resolution	Source
MWR: Microwave Radiometer	Precipitation, wind speed, sea ice concentration, water vapor	23.8 GHz and 36.5 GHz; 36.5 polari-metric; 23.8 V-pol; 390 km swath	50 km	CONAE
NIRST: New IR Sensor Technology	Hot spots (fires); Sea Surface Temperature	Bands: 3.8, 10.85 and 11.85 μm Swath: 182 km; Tilt: ± 532 km	350 meters	CONAE
HSC: High Sensitivity Camera	Urban lights; Lightning Snow cover	Bands: 490-610 μm; Swath: 700 km;	200-300 m	CONAE
DCS: Data Collection System	Environmental data collection	Band: 401.55 MHz uplink	2 contacts per day with 200 platforms	CONAE
ROSA: Radio Occultation Sounder for Atmosphere	Properties of the Atmosphere	GPS occultation	Horizontal: 300 km Vertical: 300 m	ASI (Italy)
CARMEN 1: (ICARE and SODAD)	ICARE: Effect of cosmic radiation on electronics; SODAD:	ICARE: Three fully depleted Si and Si/Li detectors	ICARE: 256 channels SODAD:	CNES (France)

	Distribution micro-particles and space debris	SODAD: Four SMOS sensors	sensitivity 0.5 μ at 10 km/s	
TDP: Technology Demonstration Package	Position, velocity and time; Inertial angular velocity	GPS receiver; Inertial reference unit	20 meters; 1 m/s; 0.2 μs; ARW: $8*10^{-3}$ deg/sqrt h	CONAE

TABLE II
Parameters of the Aquarius Mission

Orbit			**Antenna**	
Altitude	657 km		Main Reflector	2.5 m offset
Sun-synchronous	6 pm ascend		Beam look angles (deg)	25.8, 33.8, 40.3
Inclination	98 deg		Local incidence (deg)	28.7, 37.8, 45.6
Coverage	7 day global		Resolution	76x94, 84x120,
Swath	390 km			96x156 km
Radiometer			**Scatterometer**	
Frequency	1.413 GHz		Frequency	1.26 GHz
Polarization	Polarimetric		Polarization	HH, VH, HV,
Sample time	10 ms			VV
Integration time/sample	9 ms		PRF	100 Hz
NEDT (5.76 seconds)	0.06K		Pulse width	0.98 ms
Calibration Stability	0.13K		Calibration	0.1 dB

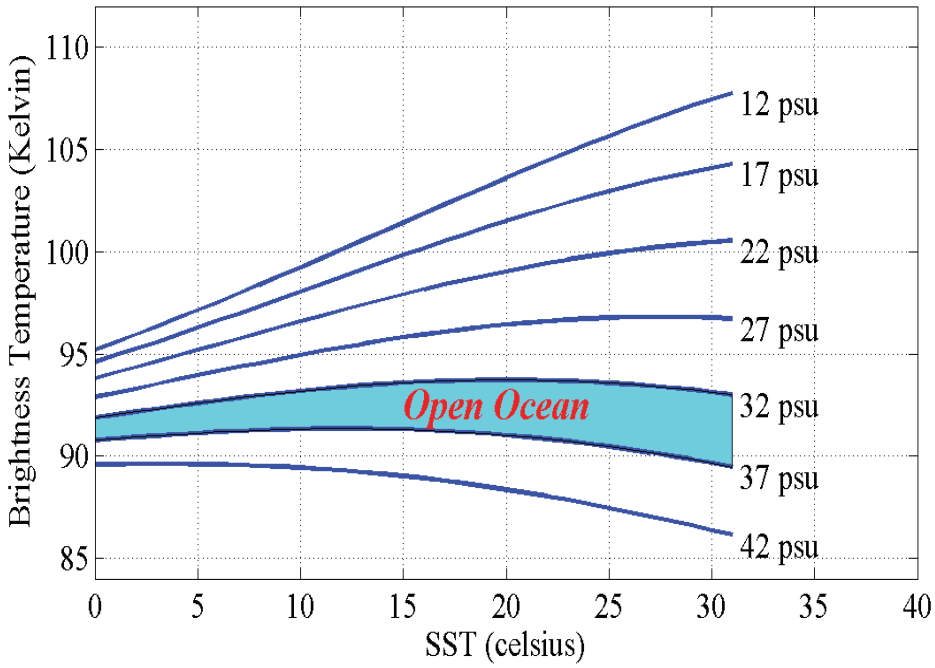

Figure 1: Level curves of constant salinity as function of sea surface temperature (abscissa) and microwave brightness temperature (ordinate) for L-band (1.4 GHz) and normal incidence.

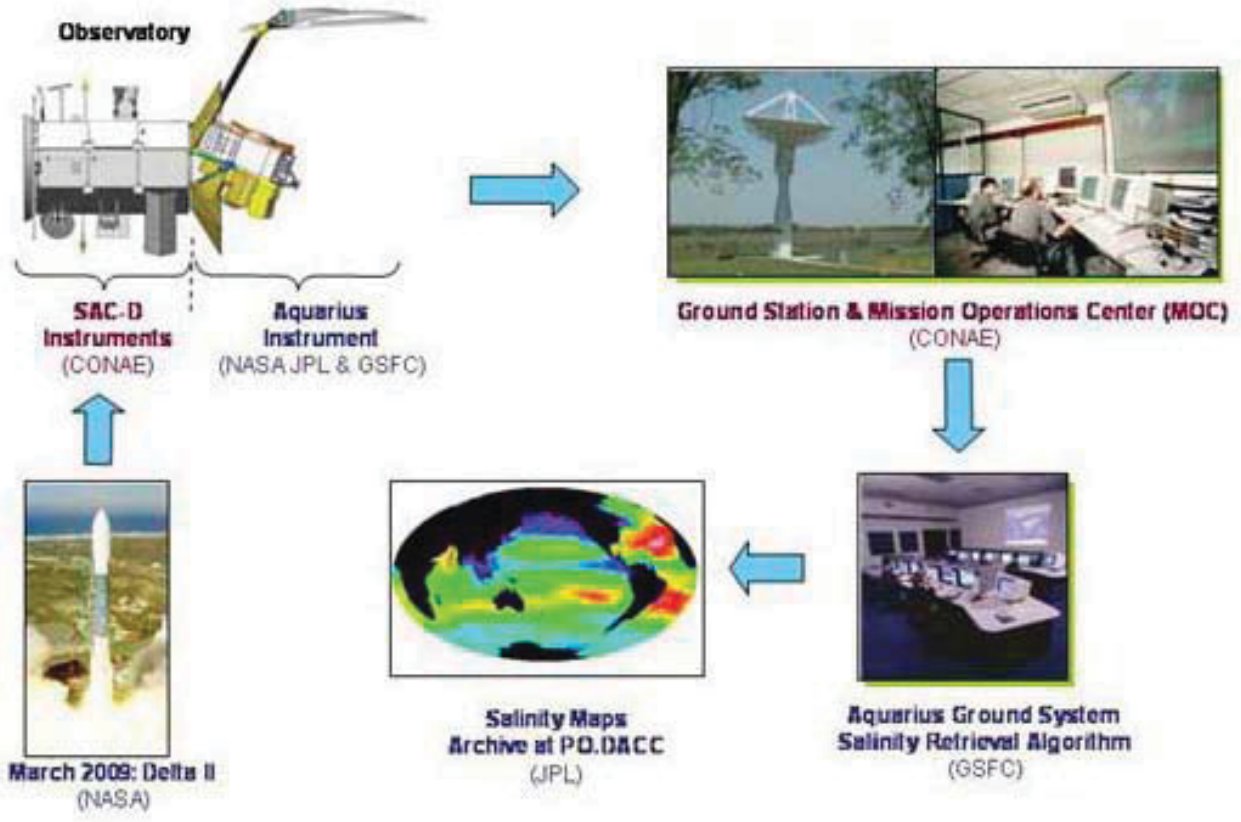

Figure 2: Schematic showing an overview of the mission and roles of the partners. Launch is from Vandenberg AFB and mission operations and the data down link is through the CONAE facilities at Cordoba. Aquarius science data is processed at the NASA's Goddard Space Flight Center and archived at the JPL PO.DAAC.

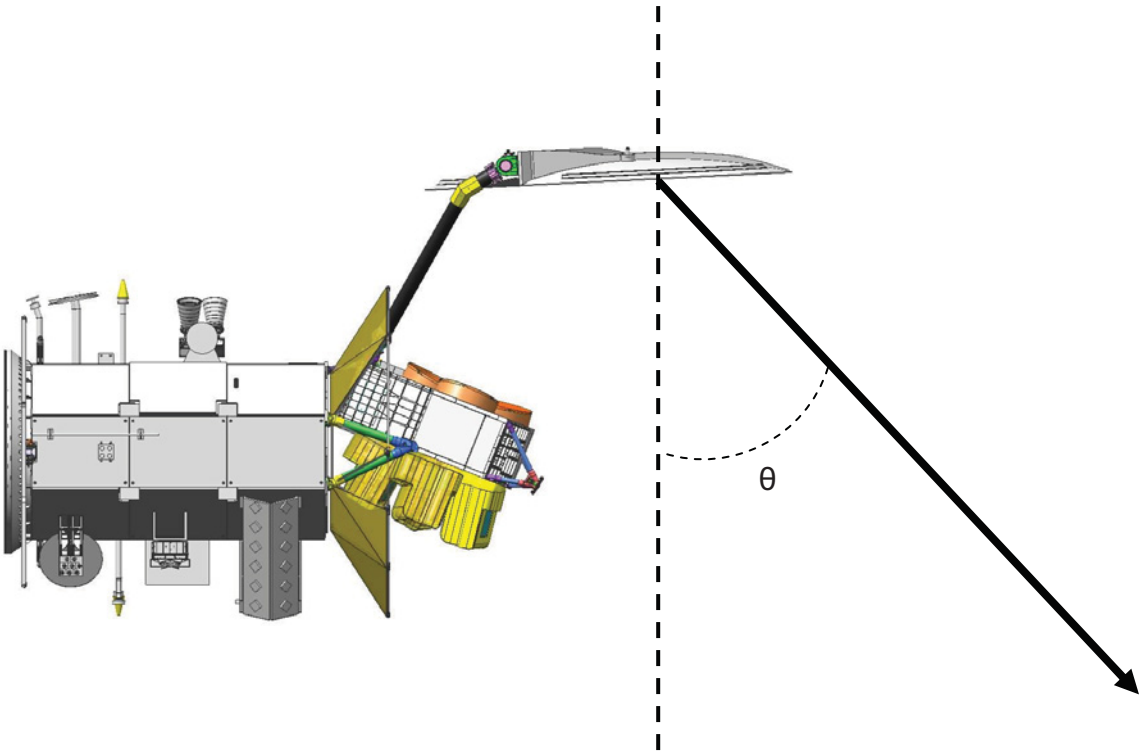

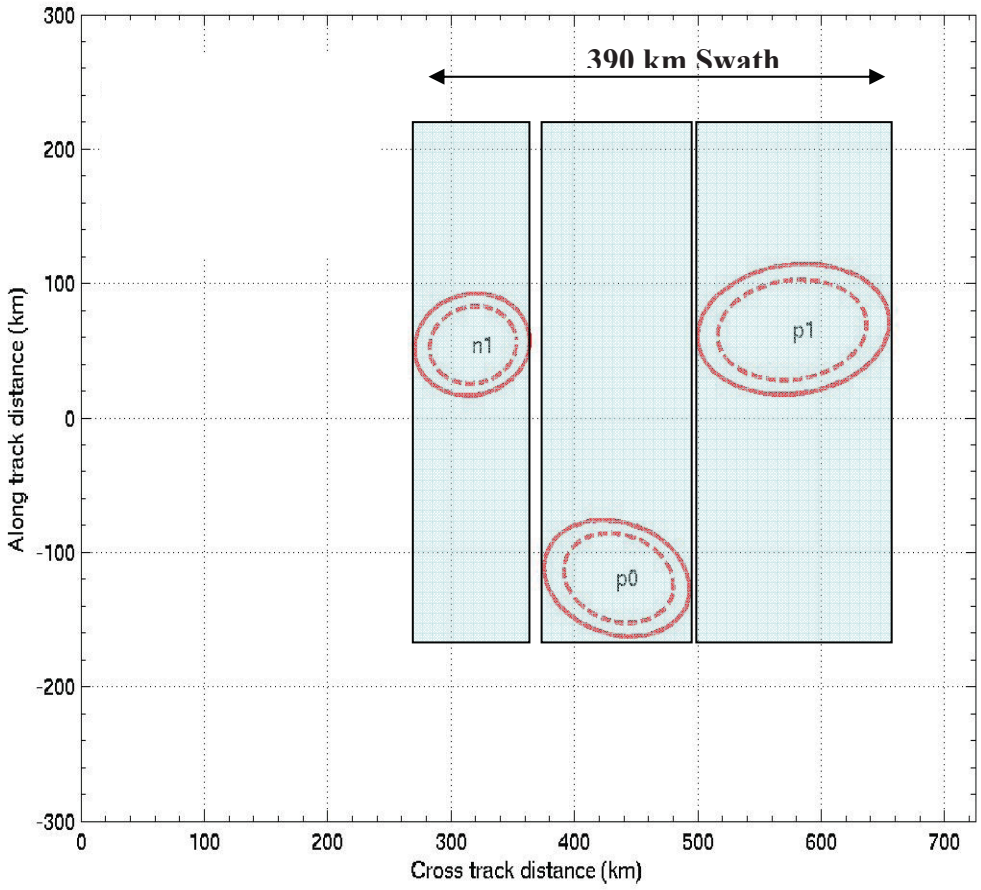

Figure 3: Aquarius (top) flying into the page and (bottom) showing the footprints and swath of the three beams. The solid lines (bottom) are the radiometer 3 dB footprint and the dashed lines show the scatterometer 3 dB footprint. The principle axes of the ellipses for the radiometer are 76 x 94, 84 x 120, 96 x 156 km and the swath is 390 km wide.

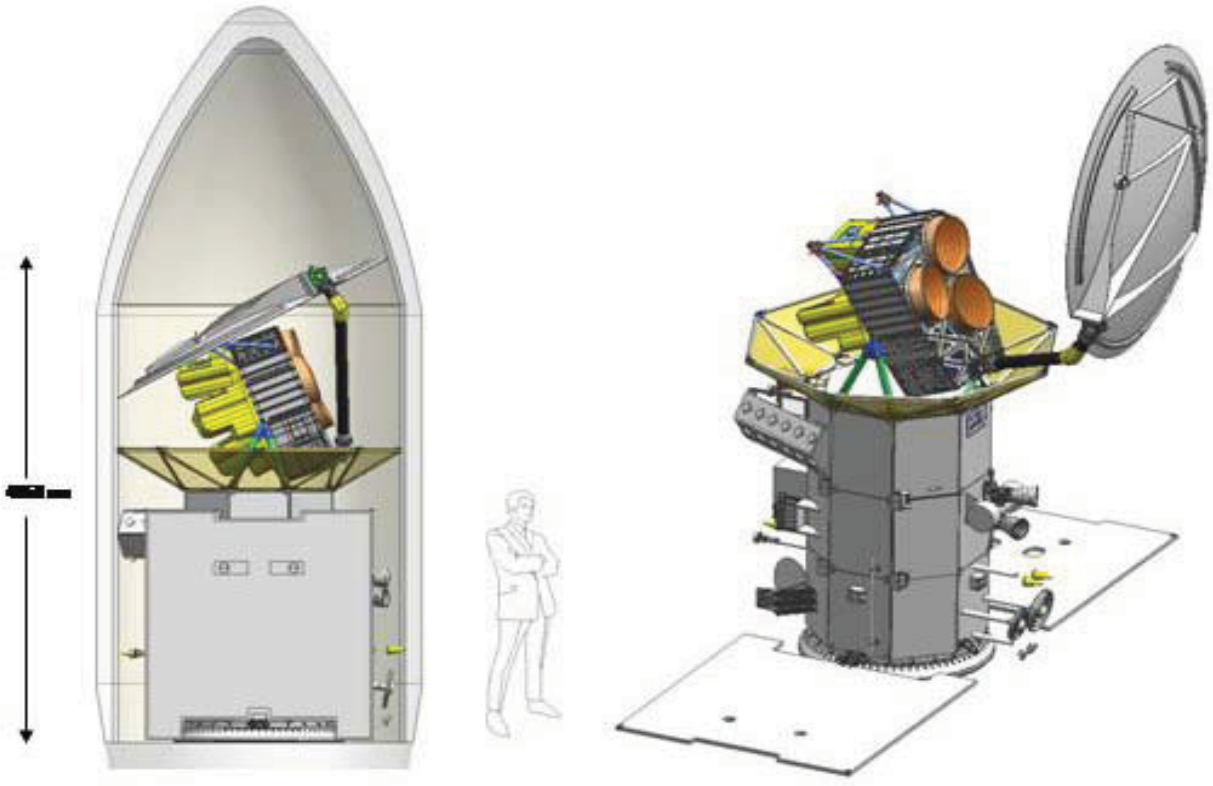

Figure 4: Aquarius in the stowed configuration (left) and deployed (right). The deployed configuration shows Aquarius mounted on the SAC-D spacecraft. The collar between the spacecraft and Aquarius instrument is a sun shade.

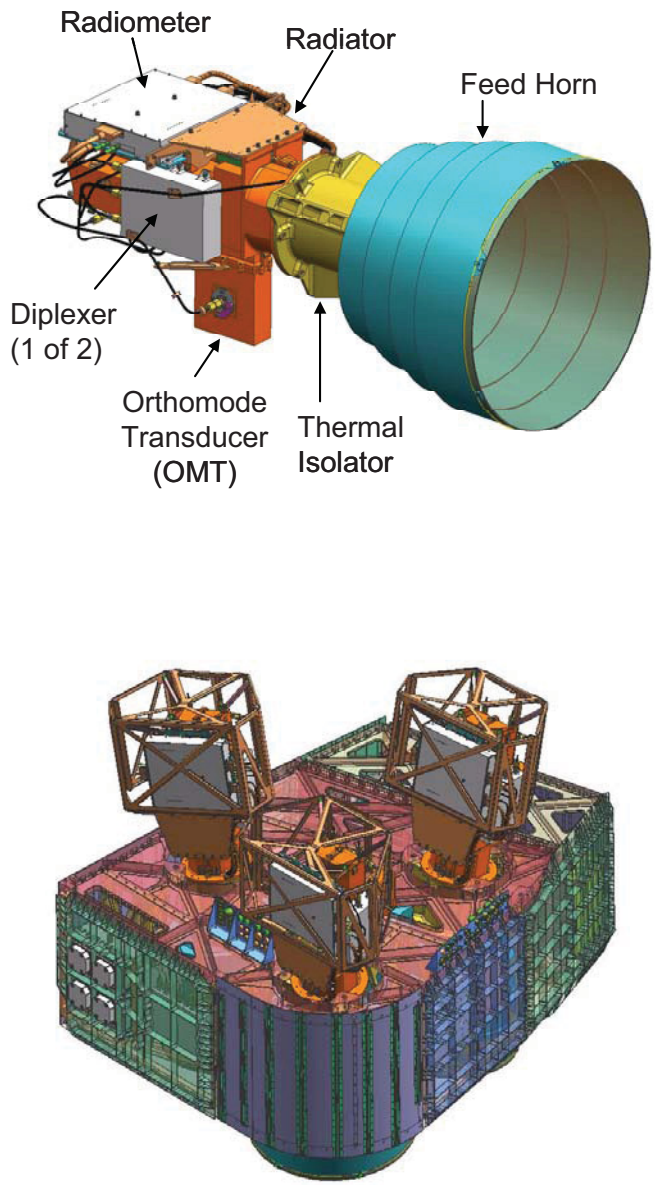

Figure 5: Aquarius feed assembly. View of the complete assembly from the back (bottom) and view of one individual feed assembly (top). Multi-layer-insulation (MLI) blankets will be attached to the cages that can be seen around each of the feed assemblies (bottom) for passive thermal control.

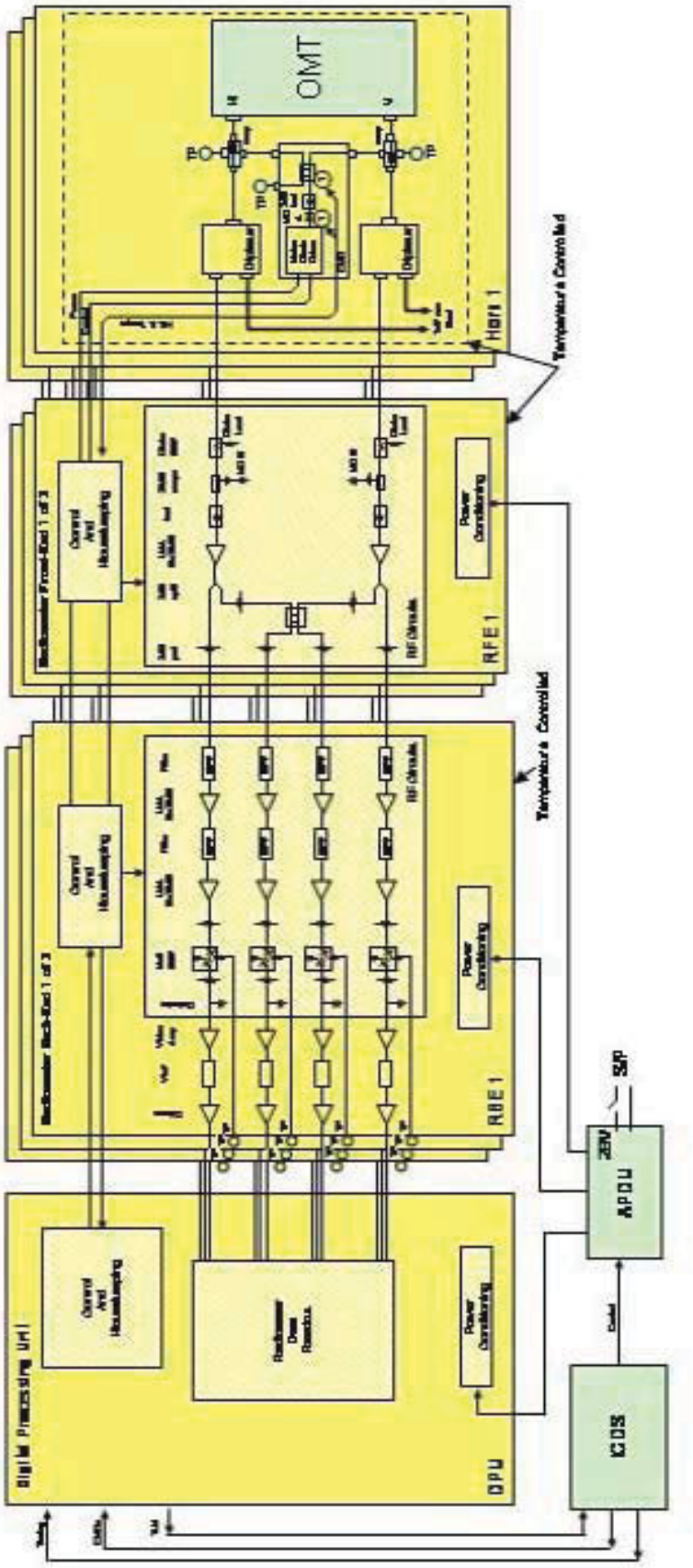

Figure 6: Radiometer block diagram showing the several radiometer elements: OMT, OMT coupler, Diplexers, Radiometer Front End (RFE), Radiometer Back End (RBE) and the Digital Processing Unit (DPU). The Aquarius Power Distribution Unit (APDU) will supply regulated DC power to all other electronics boxes. The ICDS will provide commands and handle the packaging of data from DPU and processing of data from SBE.

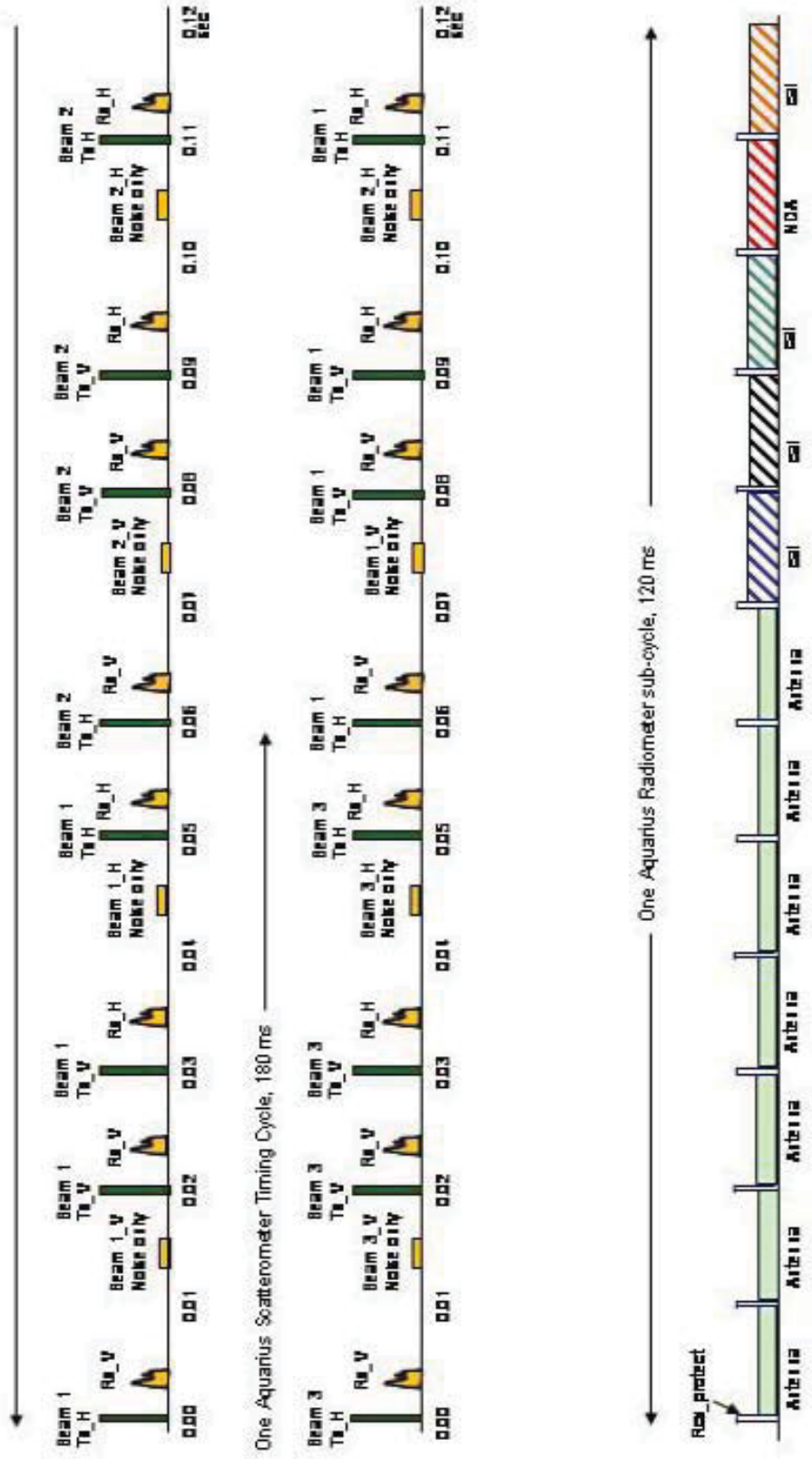

Figure 7: Aquarius instrument master timing diagram.

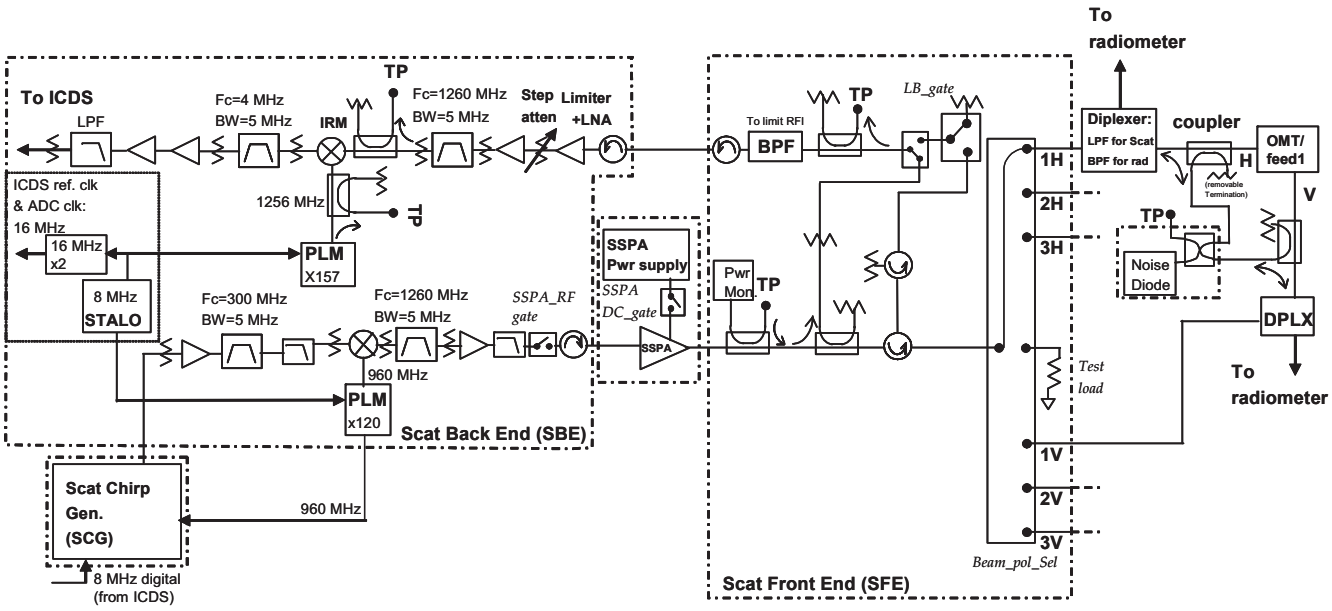

Figure 8: Scatterometer block diagram. The major elements of the scatterometer are the OMT coupler, Diplexer, Scatterometer Front End (SFE), Scatterometer Back End (SBE), Scatterometer Chirp Generator (SCG) and the Solid State Power Amplifier (SSPA).

End of File